A wide-angle seismic traverse through the Variscan of southwest Ireland

F. Masson,[1] A. W. B. Jacob,[2] C. Prodehl,[1]
P. W. Readman,[2] P. M. Shannon,[3] A. Schulze[4] and U. Enderle[1]

[1] *Geophysical Institute, University of Karlsruhe, Hertzstraße 16, D-76187 Karlsruhe, Germany. E-mail: fmasson@gpiwap1.physik.uni-karlsruhe.de*
[2] *Dublin Institute for Advanced Studies, 5, Merrion Square, Dublin 2, Ireland*
[3] *University College Dublin, Belfield, Dublin 4, Ireland*
[4] *GeoForschungsZentrum Potsdam, Telegrafenberg, Haus F, D-14473 Potsdam, Germany*

SUMMARY

A wide-angle seismic profile across the western peninsulas of SW Ireland was performed. This region corresponds to the northernmost Variscan thrust and fold deformation. The dense set of 13 shots and 109 stations along the 120 km long profile provides a detailed velocity model of the crust.

The seismic velocity model, obtained by forward and inverse modelling, defines a five-layer crust. A sedimentary layer, 5–8 km thick, is underlain by an upper-crustal layer of variable thickness, with a base generally at a depth of 10–12 km. Two mid-crustal layers are defined, and a lower-crustal layer below 22 km. The Moho lies at a depth of 30–32 km. A low-velocity zone, which coincides with a well-defined gravity low, is observed in the central part of the region and is modelled as a Caledonian granite which intruded upper-crustal basement. The granite may have acted as a buffer to northward-directed Variscan thrusting. The Dingle–Dungarvan Line (DDL) marks a major change in sedimentary and crustal velocity and structure. It lies immediately to the north of the velocity and gravity low, and shows thickness and velocity differences in many of the underlying crustal layers and even in the Moho. This suggests a deep, pre-Variscan control of the structural development of this area. The model is compatible with thin-skinned tectonics, which terminated at the DDL and which incorporated thrusts involving the sedimentary and upper-crustal layers.

Key words: crust, gravity, refraction seismic, SW Ireland.

INTRODUCTION

The Variscan orogenic region is characterized by a broad, elongate band of orogenic deformation and extends from Ireland into the UK and eastwards as far as Germany (Matte 1986). Further eastwards its continuation is less clear. The effects of Variscan deformation are clearly exposed in southern Ireland as a zone of east–west thrusts and tight, asymmetric cleaved folds. The relatively sharp northern boundary of this zone was defined by Gill (1962) as the Dingle–Dungarvan Line (DDL) and is traditionally regarded as the Variscan front (Figs 1 and 2). North of the DDL there is a rapid gradation into a zone of relatively gentle folding along ENE-trending axes with little or no cleavage even in pelitic layers. Along part of its length the DDL is marked in surface outcrop by a major Variscan reverse fault, the Killarney–Mallow Fault, which can be mapped for approximately 70 km.

The western part of the DDL is regarded by some authors (Price & Todd 1988) as the structural response to Variscan reactivation of the northern margin of the late Palaeozoic Munster Basin. Further east, however, the relationship between the DDL and the Munster Basin is less obvious, with thick Devonian clastics developed to the north of the DDL. Williams *et al.* (1989) defined another lineament (the Dingle Bay–Galtee Fault Zone) oblique to the DDL and running approximately northeastwards from Dingle Bay, and they regard this as the northern boundary of the Munster Basin. The structural significance of the Variscan frontal thrust zone south of the DDL has long been debated. Some authors (Cooper *et al.* 1984, 1986) have argued that the zone represents an area where a linked Variscan (late Carboniferous) thrust system developed above a low-angle detachment in response to northward-directed compression. This so-called 'thin-skinned' model involved detachment and northward translation of the sedimentary cover and sometimes part of the crustal basement (the depth to the
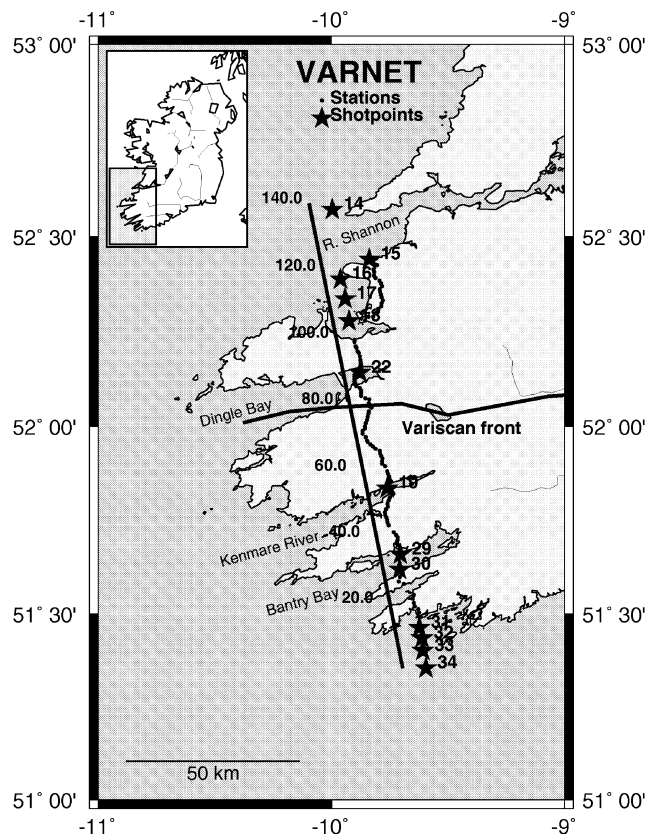
Figure 1. Location map of the VARNET seismic experiment. The black stars indicate the shots used in this study; points indicate the stations used. The labelled line parallel to the line of points indicates the distances (in kilometres) from shot 34. These distances were used during the modelling and are referred to in the discussion. The east–west-trending thick line indicates the postulated position of the Variscan front; it corresponds to the DDL.

detachment layer may vary significantly across the Variscan frontal zone). However, others (e.g. Sanderson 1984) have interpreted the area in terms of regional dextral transpression and have made a case for 'thick-skinned' deformation involving steep, non-linked faults that cut through the entire crust. The essential difference between these two structural end-members is the presence of a linked horizontal detachment, even if deep in the crust, in the thin-skinned model.

Gravity data from the region indicate a gravity low (Murphy 1960, 1974) to the south of the DDL and to the west of the Killarney–Mallow Fault. The gravity anomaly has variously been interpreted as a thick (up to 13 km) sedimentary depocentre (Emenike 1986) or as a granite complex (Howard 1975). Ford, Brown & Readman (1991) indicated that the gravity data were compatible with either a Caledonian granite body or a ductilely thickened sedimentary basin with a pre-deformation thickness of 5–6 km and a deformed thickness of at least 10 km. However, their geological arguments and hypotheses, based upon examination of the well-exposed structural features in SW Ireland augmented by gravity data, could not distinguish between the two interpretations. Hitherto, the only seismic control available to test or constrain the various contrasting geological models has been part of a wide-angle seismic profile (Lowe & Jacob 1989) which crossed the eastern part of the Variscan terrane in Ireland.

The VARNET project is a multidisciplinary study of Variscan structures in Ireland, employing wide-angle seismic data, teleseismic delay patterns, seismic crustal transfer functions, gravity data and magnetotelluric techniques to elucidate the crustal structure. The present paper is based upon a new wide-angle seismic profile (Fig. 1) acquired as part of the project. The profile was located to the west of the Killarney–Mallow Fault and crosses both the gravity low and the putative Variscan front. The objectives of the profile are to provide a crustal velocity model across the northern margin of the Variscan domain, and to investigate the nature of the gravity low and the structural style within the crust and Palaeozoic sediments across the region.

THE SEISMIC PROFILE

The seismic profile crosses the westernmost peninsulas of Ireland, extending from Roaringwater Bay in the south to the estuary of the River Shannon in the north (Figs 1 and 2). During the experiment, 109 stations were deployed at about 1 km intervals and 13 shots were fired. The total length of the line, including off-end shots, was about 140 km, although the maximum shot-to-station distance was about 120 km.

A series of sea inlets made it possible to fire quite small shots (25 or 50 kg) in water at intervals along the line, with sequences of shots at each end. The interleaving of shots and stations along the line provided dense, overlapping ray paths and good control on crustal structure. Approximately 1300 three-component seismograms were recorded and all the digital data were at 100 samples per second.

THE SEISMIC SECTIONS

Figs 3–7 show the record sections for *P* waves, with the phase traveltimes computed from the model shown in Fig. 8. Fig. 9 shows the ray paths used for the modelling. The model is composed of six layers, from near the surface to the upper mantle below the Moho. A very thin and variable surface layer is not included in the numbering of the layers and phases. The *Pi*1 phase is the wave diving through the first layer (often called the *Pg* phase) (Fig. 9), *Pi*1*P* is reflected from the top of the second crustal layer, *Pi*2 is the refracted wave travelling through the second crustal layer, etc. *PmP* is the phase reflected from the Moho. The phases that have been clearly identified are *Pi*1, *Pi*1*P*, *Pi*2, *Pi*2*P*, *Pi*3*P*, *Pi*4*P* and *PmP*. As the maximum shot-to-station distance was 120 km, first arrivals from the uppermost mantle (*Pn*) were not observed. The distance at which *Pn* is expected to become a first arrival is between 130 and 140 km in this region.

All record sections in this paper are vertical-component ones, plotted with a reduction velocity of 6 km s^{-1} and normalized to a standard maximum amplitude for each trace. They were all bandpass filtered between 2 and 30 Hz. The frequency content varies from section to section, as the depth of water at the shot points varied. The dominant frequency and the signal amplitude are strongly affected by the water depth (Jacob *et al.* 1994). The shots are described in Table 1.

The appearance of the sections varies quite significantly along the profile so the sections have been put into five groups, each containing one or more sections recorded from shots in one of the five bodies of water along the profile. These groups are discussed below, and a summary of the phases observed
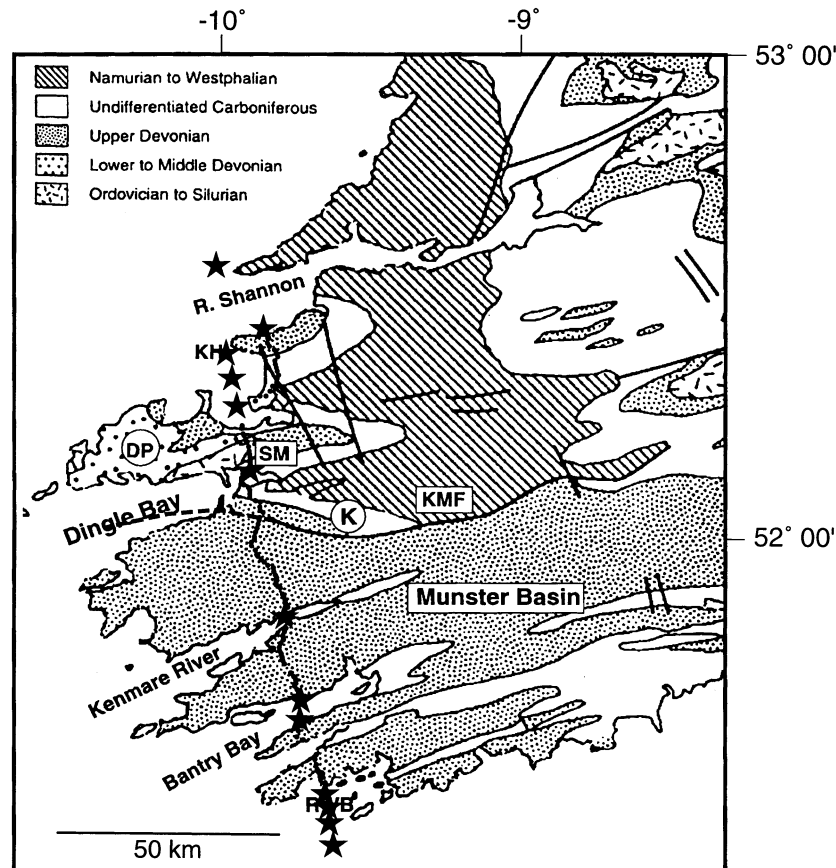
Figure 2. Simplified geological map of the area. Mapped faults are shown as thick lines. KMF, Killarney–Mallow Fault; SM, Slieve Mish; K, Killarney town; KH, Kerry Head; DP, Dingle Peninsula; RWB, Roaringwater Bay.

in each section is shown in Table 2. Phases which are observed in each section are shown in Figs 3–7 by continuous lines, while phases which are predicted by the model, but not observed, are shown by dashed lines.
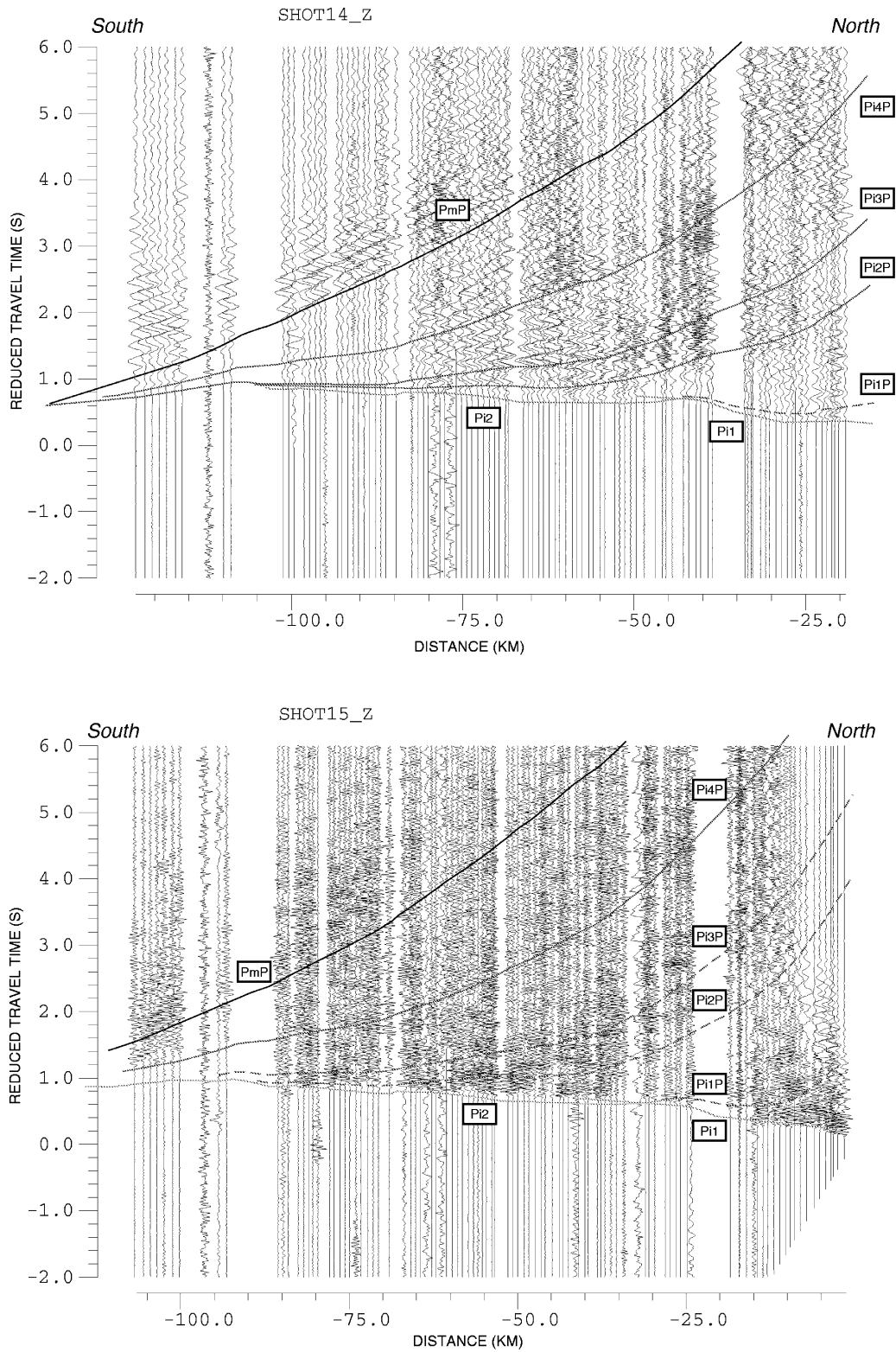
Northern group (shots 14–18)

Four phases can be seen in the record sections 14 and 15 (Fig. 3): the direct wave $Pi1$, the diving wave through the second layer ($Pi2$), a deep crustal reflection ($Pi4P$) and the PmP reflection from the Moho. The clearness of the PmP phase decreases from shot 14 to shot 15 and becomes very weak on sections 16–18. In the same way, the fit of the $Pi4P$ phases is less convincing for shots 15–18. Section 16 shows clear secondary arrivals before $Pi4P$, between 65 and 80 km, which are reflections from the top of the fourth layer. This $Pi3P$ phase is weakly visible on sections 14 (-60 to -80 km) and 18 (-75 to -90 km). The $Pi2P$ phase from the top of layer 3 is observed on section 14 (-60 to -80 km) and weakly on section 15 (-65 to -80 km). It is impossible to fit the phases identified as $Pi2P$ and $Pi3P$ with only one interface, even if the layer between the second and the third interfaces is very thin. The reflection from the base of the first layer ($Pi1P$) is clearly identified in the northern part of section 18 and can also be recognized on record sections 16, 17 and 18. This set of record sections shows the complexity of the deep crustal and Moho reflections. The phases have emergent onsets and strong codas.

Shot 22 (Dingle Bay)

In the southern part of the record section, the first arrivals beyond 18 km are very weak (Fig. 4). This is taken into account in the model, since the calculated $Pi1$ phase is not defined beyond -20 km. In order to explain this feature, a very thin high-velocity layer has been introduced into this model at the top of a low-velocity zone (see Fig. 8) around 85 km. This sharp change in structure is located close to the area where the seismic profile crosses the DDL. $Pi2P$ and $Pi4P$ can also be identified on the southern section. $Pi2P$ is visible from -27 to -52 km and disappears at -60 km. $Pi2P$ has a strong coda, which may mask $Pi3P$. In the same way, $Pi4P$, visible from -25 km up to the end of the profile, obscures the PmP phase. The first arrivals of the northern part of the section show at least three complex features marked by strong signals (between 5 and 10 km, 20 and 25 km, and 27 and 32 km). The P-wave model does not fit these features but the calculated $Pi1$ phase fits closely the general trend of the first arrivals. Another strong-energy phase is visible on the section between 15 and 32 km, corresponding to $Pi2P$.

Shot 19 (Kenmare River)

On this record section (Fig. 5), a new feature appears which is observed on all of the more southern record sections. This feature is an abrupt change in the first arrivals and it coincides with the DDL (at about 30 km on this record section). Towards

Figure 3. Trace-normalized *P*-wave record sections for the five shots of the northern group (shots 14–18). The data have been bandpass filtered from 2 to 30 Hz. All record sections are vertical-component sections, plotted with a reducing velocity of 6 km s^{-1}. Superimposed are the traveltimes computed from the *P*-wave model shown in Fig. 8 by ray tracing (dashed lines indicate the unclear phases). The *Pi*1 phase represents the wave diving through the first layer (classically named the *Pg* phase), *Pi*1*P* the wave reflected from the top of the second crustal layer, *Pi*2 the refracted wave travelling through the second crustal layer, etc. *PmP* is the wave reflected from the Moho (see also Fig. 9).
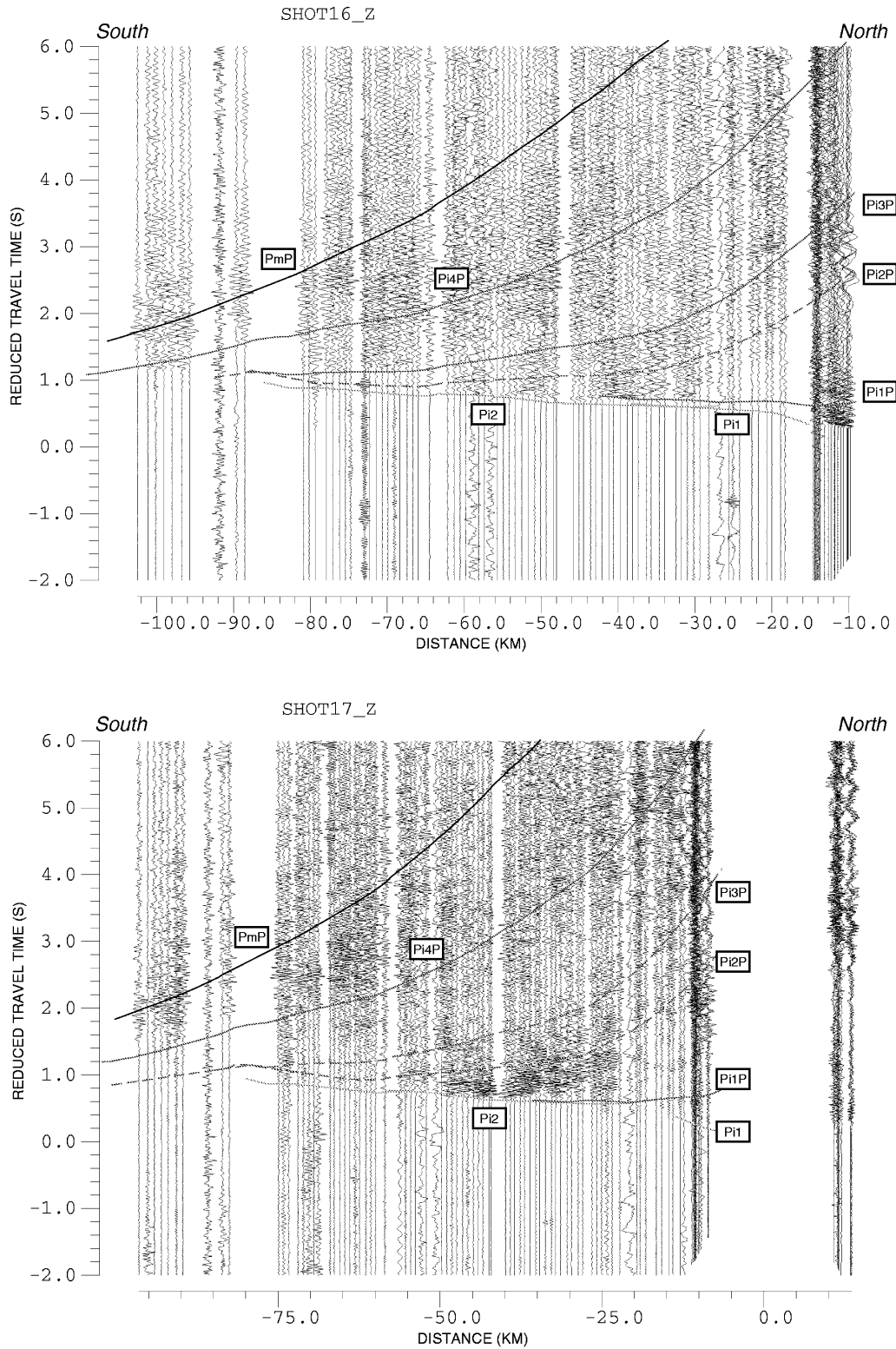
Figure 3. (*Continued.*)

the north, the first arrivals are well marked from the shot point up to 31 km and correspond to *Pi*1. Then they lose energy, especially between 33 and 43 km. Beyond this distance, the first observed arrivals fit the *Pi*2 phase. Between 15 and 30 km, a strong-energy coda is identified as *Pi*1*P*. *Pi*2*P* can be associated with a weak arrival from 37 to 60 km which

strengthens beyond 60 km. *Pi*4*P* may exist as a strong but very emergent phase which does not give precise information on either the depth of the interface or the velocity above it. The southern part of the profile shows strong first arrivals, well fitted by *Pi*1, while *Pi*2*P* is clearly observed to the end of the profile. *Pi*1*P* fits a weak phase between −32 and −38 km.
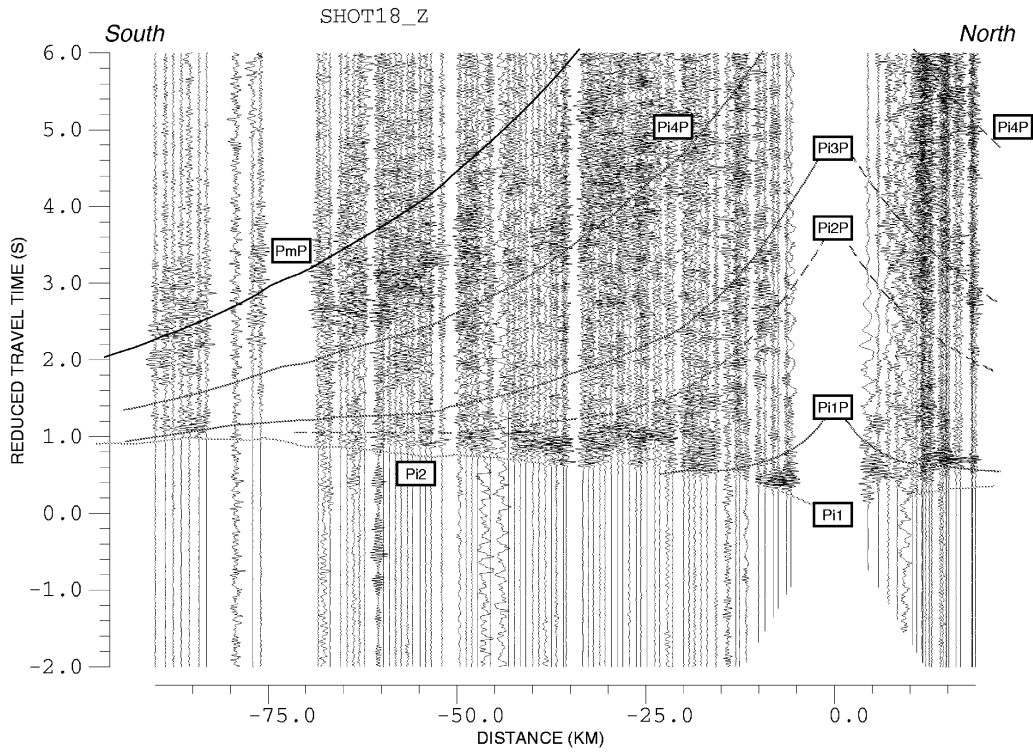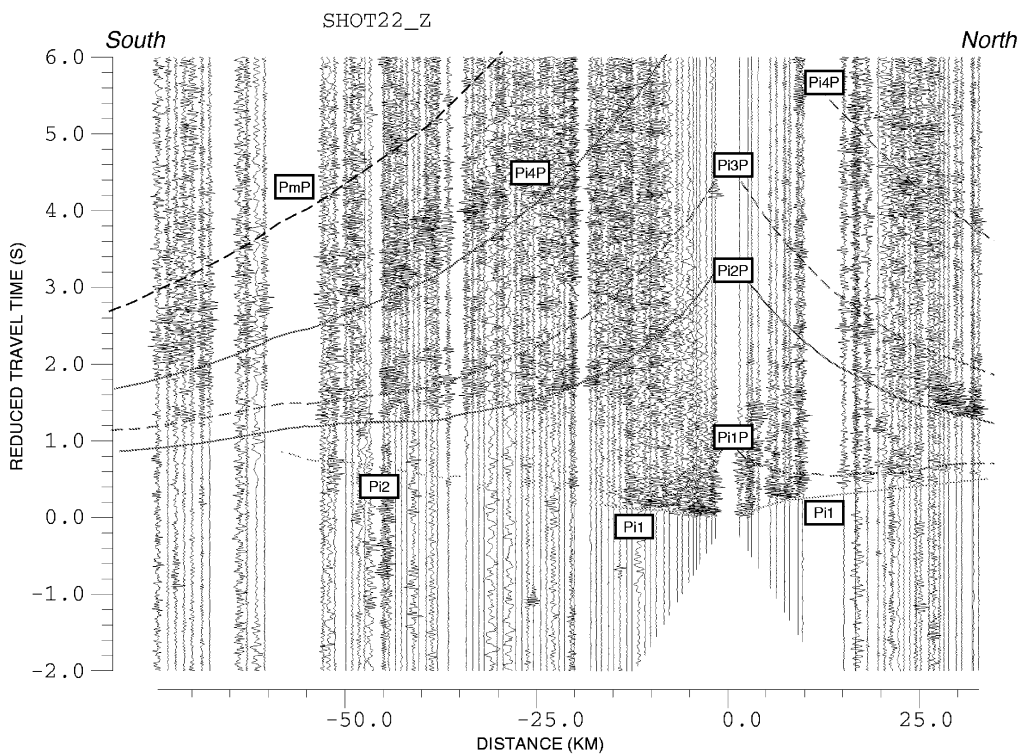
Figure 3. (*Continued.*)

Figure 4. Record section for shot 22 (Dingle Bay), as in Fig. 3.

Bantry Bay (shots 29 and 30)

The main feature of these two shots is again an abrupt change of the first arrivals near the DDL (Fig. 6). For both shots, the strong first arrivals are well fitted by *Pi*1 up to this zone (48 km for shot 29, 53 km for shot 30). The variation of the offset of this abrupt change, the same as the separation between the two shots, confirms that this feature is due to a variation in the structure in a particular zone and not to a vertical velocity variation. Beyond this zone, the first arrivals correspond to
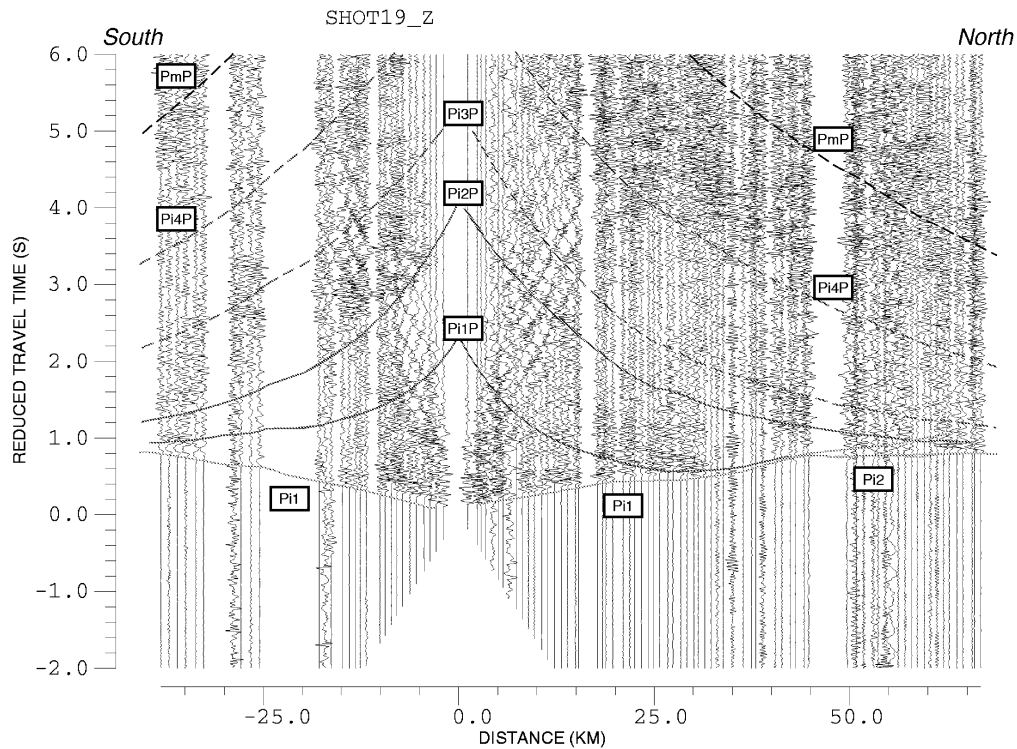
© 1998 RAS, *GJI* **134,** 689–705

Figure 5. Record section for shot 19 (Kenmare Bay), as in Fig. 3.

*Pi*2. The pattern of first arrivals on either side of the zone is taken into account in the model and fitted by phases *Pi*1, *Pi*2 and *Pi*1*P*, especially for shot 30. *Pi*1*P* again has a strong coda. The identification of phases *Pi*2*P*, *Pi*3*P* and *Pi*4*P* is more difficult, because of the number of arrivals between 50 km and the end of the profile. On section 30, there is a clear *PmP* phase. To the south, only the first arrivals, fitted by the phase *Pi*1, are identifiable.

Southern group (shots 31–34)

These four shots (Fig. 7) were fired on a line about 12 km long and the patterns in these sections show some significant variations, although they all have a discontinuity at the DDL. The first arrivals here, between about 70 and 80 km, are successively fitted by the phases *Pi*1, *Pi*2 and *Pi*1*P* for shots 31 and 32, and *Pi*1 and *Pi*2 for shots 33 and 34. Beyond, the first arrivals disappear for about 20 km. The end of the profile is more confused. For all the shots, for about 10 km around 100 km, the first arrivals are fitted by *Pi*2 and/or *Pi*2*P*. Then the first arrivals disappear again, become very weak (shot 32), or are reasonably well fitted by *Pi*3*P* (shots 31, 33 and 34). The *Pi*2*P* phase is clear on all four record sections. The *Pi*1*P* phase is weakly observed just behind *Pi*1 and is hard to separate from the first arrival.

Beyond the DDL, *Pi*3*P* is clearly observed on record sections 31 and 32, but only weakly on record sections 33 and 34. *Pi*4*P* is difficult to describe. On record section 31 beyond 92 km, section 32 beyond 88 km, section 33 beyond 90 km and section 34 beyond 96 km, a phase can be identified as *Pi*4*P*. In some places it is quite clear. Between the DDL and these segments, the patterns of the record sections are unclear. It seems that there is weak energy on all these sections at about the right time. In

sections 31, 32 and 33 it is followed by complexities before *PmP*, while the generally lower-frequency coda of *Pi*4*P* in section 34 may obscure some of the detail. The clearest *PmP* phase is observed for shot 32. In comparison with the northern shot points, there is only a short distance range where the *PmP* phase can be seen. The correlation of *PmP* on sections 31, 33 and 34 is problematic and complex. On these sections, there may even be a further phase (*Pi*5), but as this would only concern this group of shot points, it has not been modelled. Overall, because of the complexity in sections 31, 33 and 34, it was decided to follow the correlation in section 32.

INTERPRETATION TECHNIQUES AND VELOCITY MODEL

Techniques

There were three major steps in the modelling procedure. First, the observed phases were correlated on each record section and 1-D velocity–depth functions were calculated for the five groups of shots described above. The results of the 1-D modelling were mapped into a preliminary 2-D cross-section, making due allowance for offsets in the different phases. Next, the data were interpreted by 2-D forward modelling, initially using the structure deduced from the 1-D modelling. The ray-tracing program MacRay (Luetgert 1992) was used. Finally, when the velocity model obtained by forward modelling was good enough to identify confidently arrivals with phases, a traveltime inversion was carried out using the method of Zelt & Smith (1992). The model shown in Figs 8 and 10 is the final model obtained using a Zelt & Smith (1992) inversion.
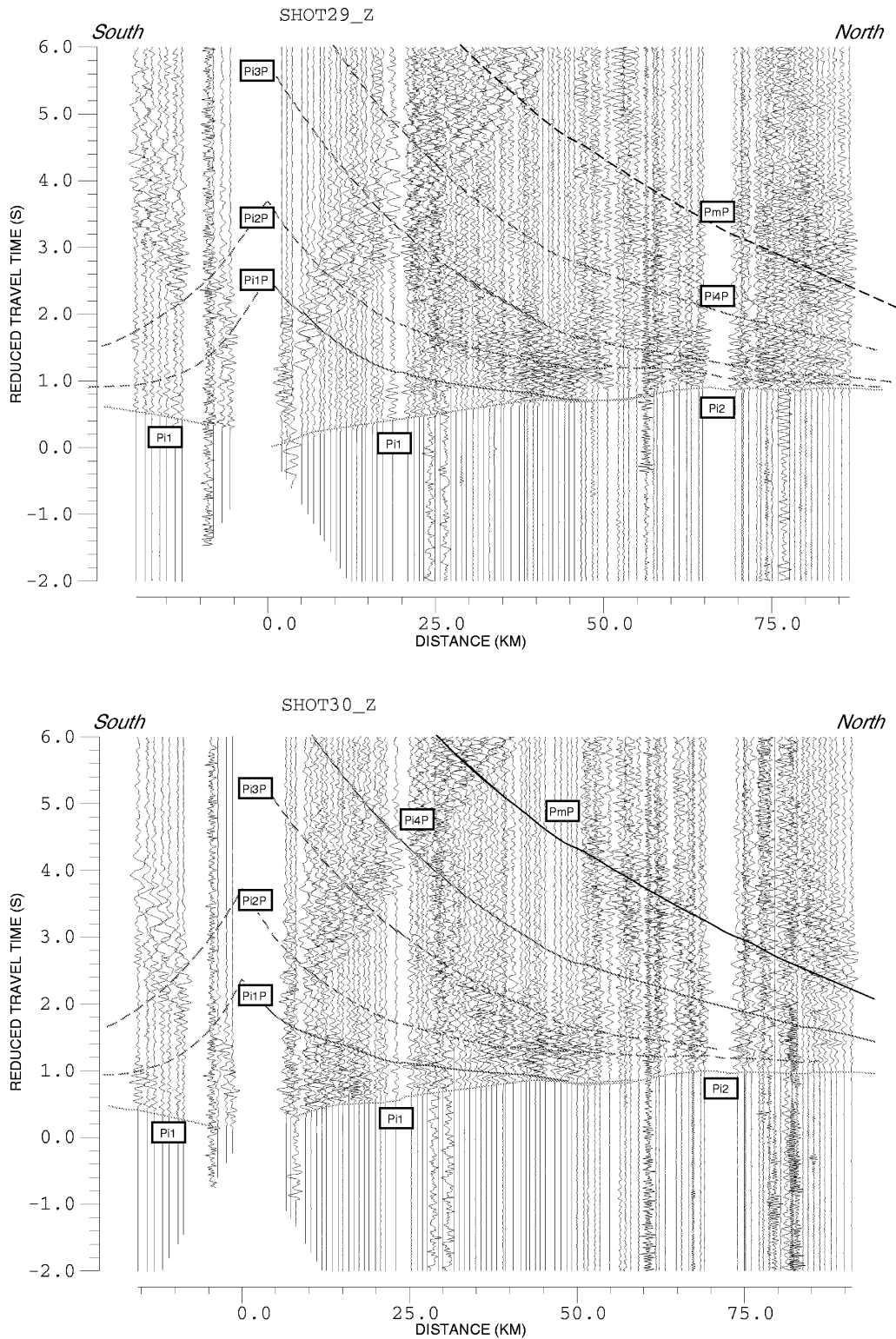
Figure 6. Record sections for shots 29 and 30 (Bantry Bay), as in Fig. 3.

Velocity model (Fig. 9)

While the model is more complex than that derived by Lowe & Jacob (1989), some comparisons can be made with the COOLE profile about 150 km to the east.

Near-surface velocity structures

A thin layer of variable thickness is included at the surface, mainly as a static correction, to fit variations in the *Pi*1 phase. However, in some cases this has geological significance. The
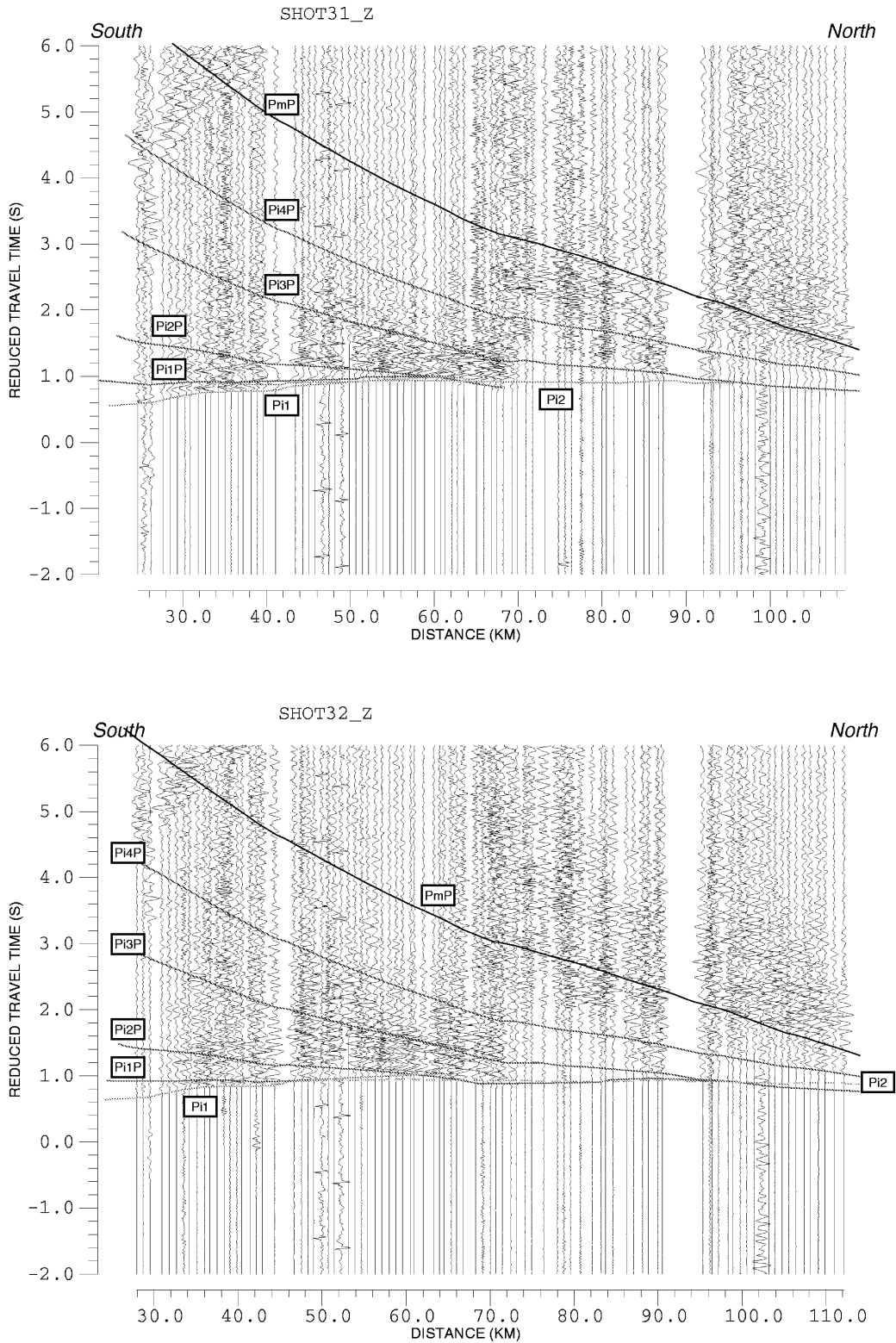
Figure 7. Record sections for shots 31–34 (southern group), as in Fig. 3.

first layer, underneath the thin, low-velocity near-surface layer, is composed of upper-Palaeozoic sediments. It is divided into two parts, separated by a horst-like structure in the second layer at about 80 km. The southern part is about 7.5 km thick, while the northern part is only about 4 km thick. The thickness decreases to less than 1 km above the horst. In the south, the vertical velocity gradient is roughly constant from 0 to 45 km (5.3 km s^{-1} at the top to 5.75 km s^{-1} at the bottom of the layer). At the other end of the profile, from 110 to 140 km, the velocity is again homogeneous (5.7–5.9 km s^{-1}). However,
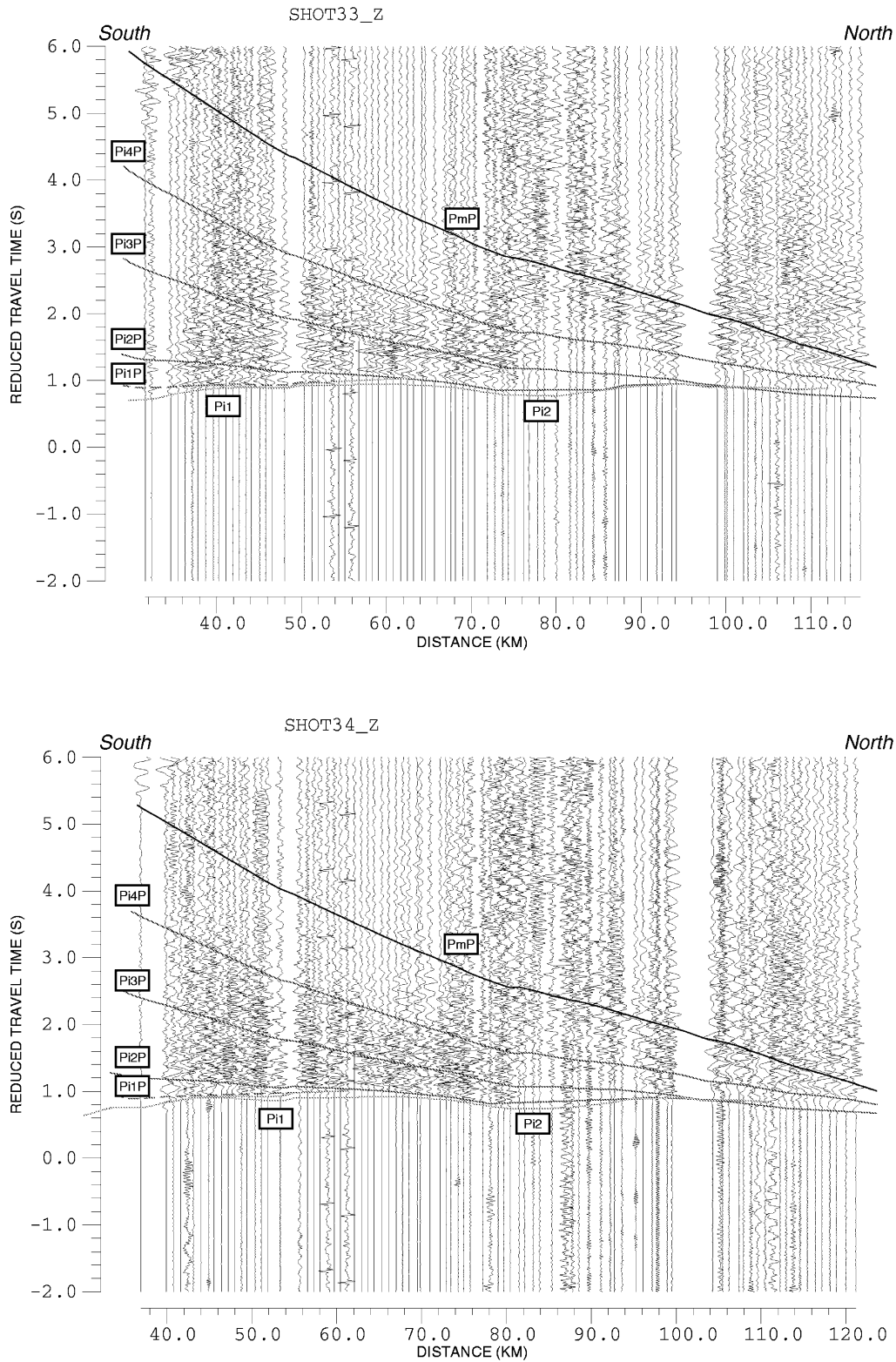
Figure 7. (*Continued.*)

from 45 to 110 km the velocity pattern is more complex, with alternating high- and low-velocity zones symmetrically around the break at 80 km.

The second layer, the upper-crustal crystalline basement, varies in thickness from south to north, but on average its base is at about 10 km depth. The main velocity feature of the second layer is a low-velocity zone, about 5.4–5.85 km s^{-1}, located where its upper surface is shallowest. This low-velocity zone, with a lateral extension of about 25 km, is bordered by two higher-velocity zones, 6.03–6.17 km s^{-1} at its southern

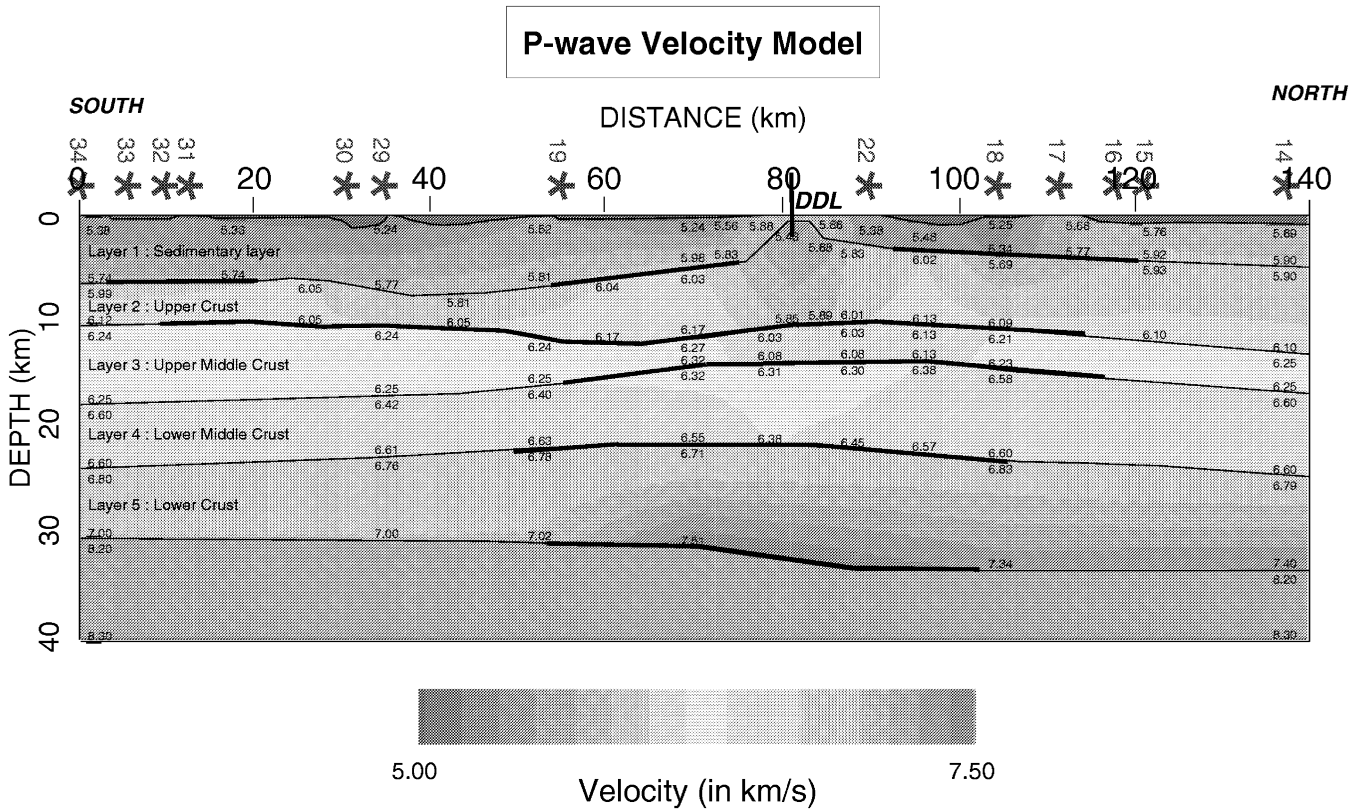**Figure 8.** 2-D velocity model. The numbers within the model show the *P*-wave velocities in km s^{-1}. The thick lines indicate the location of the observed reflections.
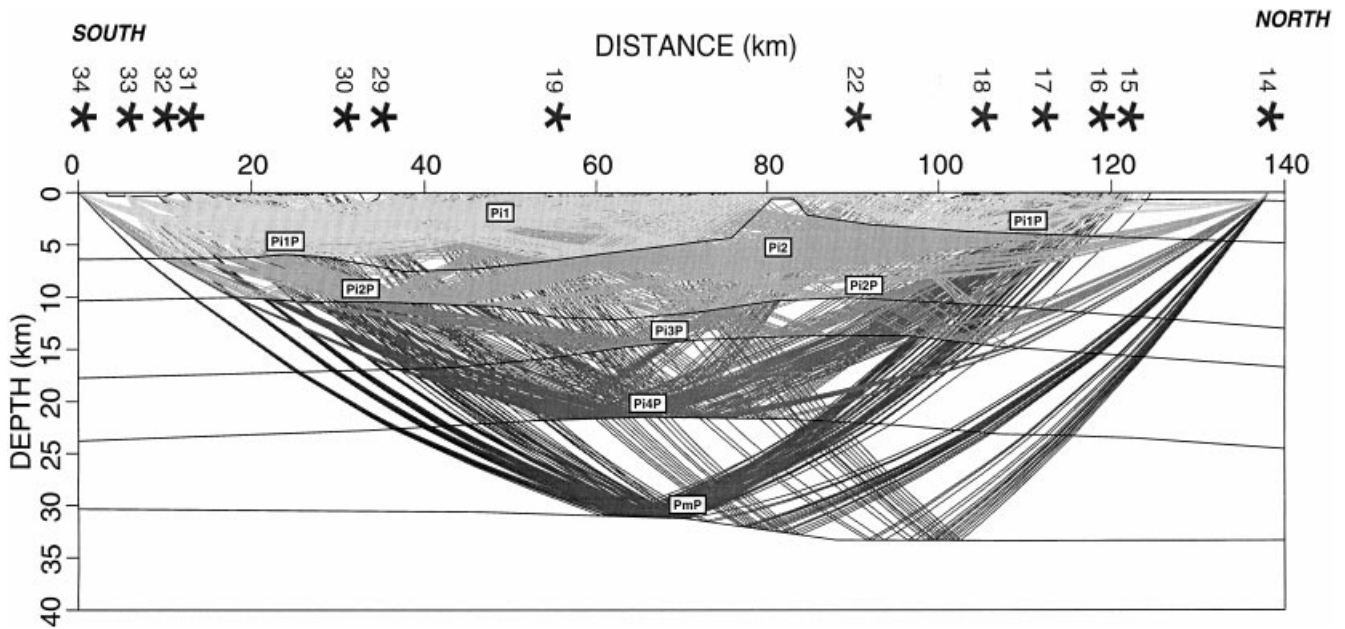
Figure 9. Ray paths of the data used in the modelling. A high ray coverage is obtained through the two shallower layers (refracted waves *Pi*1 and *Pi*2, reflected waves *Pi*1*P* and *Pi*2*P*). At greater depth the ray coverage decreases (*Pi*3*P*, *Pi*4*P* and *PmP*) and only the central part of the model is resolved.

Table 1. Location and depth of the shot points.

Shot	Latitude (°N)	Longitude (°W)	Depth (m)
14	52.5706	−09.9962	−64.0
15	52.4408	−09.8389	−16.0
16	52.3888	−09.9623	−29.0
17	52.3365	−09.9418	−15.0
18	52.2785	−09.9242	−12.0
19	51.8356	−09.7615	−17.0
22	52.1421	−09.8782	−05.0
29	51.6599	−09.7042	−38.0
30	51.6197	−09.7083	−41.0
31	51.4635	−09.6226	−42.0
32	51.4352	−09.6112	−45.0
33	51.4019	−09.6082	−54.0
34	51.3547	−09.5949	−64.0

Table 2. Summary of the phase correlation. XXX indicates an easy correlation of the phase, XX a difficult correlation and X a very difficult correlation.

	Pi1	Pi1P	Pi2	Pi2P	Pi3P	Pi4P	PmP
14	XXX		XXX	X	X	XX	XXX
15	XXX		XXX	X		XXX	XX
16	XX	X	XXX		XXX	XXX	XX
17	XX	X	XX			XXX	X
18 N	XXX	XXX					
18 S	XXX	XX	XXX		XXX	XXX	X
22 N	XXX			XXX			
22 S	XXX			XXX		XX	
19 N	XXX	XX	XX	X			
19 S	XXX	XX		XX			
29 N	XXX	XX	XX	X			
29 S	XXX						
30 N	XXX	XX	XX	X		X	XX
30 S	XXX						
31	XXX	X	X	XXX	XX	XXX	XXX
32	XXX	X	X	XXX	X	XXX	XXX
33	XXX	X	X	XXX	XX	XX	XX
34	XXX		X	XXX	X	X	X

boundary and 6.02–6.13 km s^{-1} at its northern boundary. Around 42 km and 100 km, slightly lower velocities are found near the top of the layer. The general pattern of the sediments and upper crust is broadly similar to that found by Lowe & Jacob (1989) further east.

Mid-crustal velocity structures

The middle crust comprises layers 3 and 4, which have an average total thickness of about 13 km. Layer 3 thins between 0 and 50 km (to only 3.5 km) and layer 4 thickens north of 85 km (to 7 km). The velocity is constant from 0 to 65 km and from 100 to 140 km (6.25 km s^{-1}) and decreases between 60 and 100 km, with a minimum value of 6.05 km s^{-1} at 80 km. Layer 4 shows larger velocity variations, but with the same trend as in layer 3. In the southern part of the model (20–65 km), the velocity increases from 6.4 km s^{-1} at the top to 6.6 km s^{-1} at the bottom, but decreasing slightly northwards towards the 80 km distance. Further to the north, the velocity increases again and is constant from the top to the bottom of the layer at 6.6 km s^{-1}. The mean thickness of this layer is

about 6 km in the south and 8 km in the north. These two layers are less heterogeneous than the shallower ones, even allowing for a low-velocity zone in the central part of the model. The highly variable pattern of the two first layers is not repeated.

The general pattern of this middle crust is again comparable to that of the middle crust obtained by Lowe & Jacob (1989), though their model is less detailed, a consequence of greater station spacing. They found a mean thickness of 11 km and a mean velocity of 6.4–6.5 km s^{-1}. This value is comparable to the values obtained in the northern and southern parts of this profile. The velocities in the central part of this model are lower.

Lower crust and crust–mantle boundary

The velocities in the lower crust show slight variations in its upper part and more marked variations near the Moho. The velocity in the top of the layer, at about 23 km depth, varies between 6.7 and 6.8 km s^{-1}, similar to the velocity of 6.85 km s^{-1} obtained by Lowe & Jacob (1989). At the base of the lower crust, however, velocities vary from 7.0 to 7.5 km s^{-1}. From 30 to 60 km, the depth of the Moho (30 km) and the velocity of 7.0 km s^{-1} observed just above it are in good agreement with Lowe & Jacob (1989). The Moho deepens by about 3 km between 70 and 90 km and the velocity just above it increases to 7.5 km s^{-1} below the low-velocity zone observed in the upper layers.

Uncertainties in depth and velocity

Prior to attaching any geological significance to the velocity model, an estimate of the reliability of the model is required. Errors are cumulative and there will be greater uncertainty in the deeper parts of the model than near the surface. Qualitatively, it is obvious that velocities derived from refracted phases (Pi1 and Pi2), which are easily identified and picked, are certainly reliable. Therefore, the velocities of the first two layers can be interpreted with confidence, and particularly the velocity of the horst-like structure. Velocities derived from reflected waves (i.e. the velocities of the layers 3, 4 and 5) are certainly less reliable.

The reliability of the depth to a reflector strongly depends on the number of shots generating rays and the number of rays reflected from this interface. Fig. 8 shows the segments of the interfaces where waves observed on the record sections have been reflected. This is a first qualitative estimation of the reliability of the model. It appears that the second interface at about 11 km depth is the best-constrained structure. The deeper interfaces (top of the lower crust and Moho) are, according to the ray-path distribution (Fig. 9), only defined in the central part of the model. However, there is wider control of the velocity distribution as a result of oblique ray paths in the lower crust.

Two different tests were made to estimate the errors quantitatively. The first test involved a stepwise decrease and increase of the depth of a given reflector to determine the amount of vertical movement possible before changes in the calculated traveltimes became unacceptable in comparison with the observed traveltimes. The result is presented in Table 3. We shifted the second interface by amounts ranging from -1000 m to $+1000$ m and estimated the effect of this shift on the computed root mean square (RMS) traveltime. The change in

© 1998 RAS, *GJI* **134**, 689–705

P-wave Velocity Model : Resolution
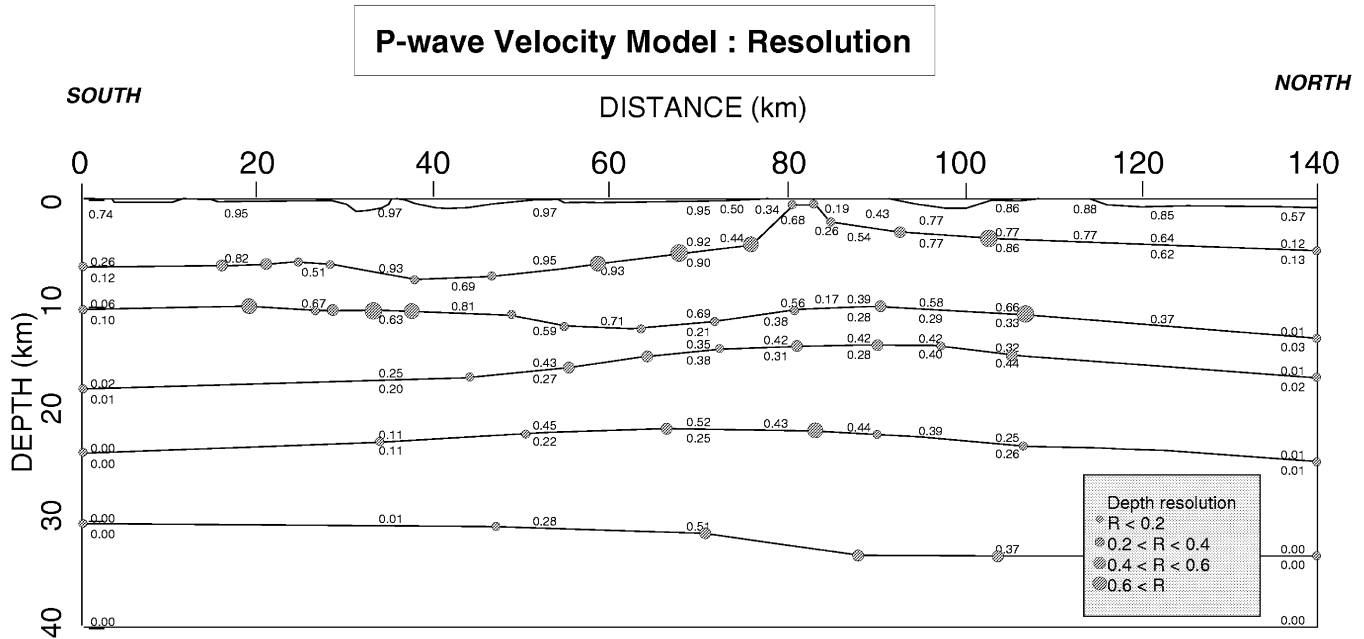
Figure 10. Diagonal elements of the resolution matrix of the inversion of traveltimes. Two sets of parameters were inverted simultaneously: the velocity and the depth of the boundary nodes. The velocity resolution is indicated by numbers, while the boundary depth resolution is indicated by sizes of circles. A value close to unity indicates a well-resolved parameter; a low value ($\ll 1$) denotes a poorly resolved parameter.

Table 3. RMS traveltime residual (Time−RMS) with respect to the observed data, calculated for rays reflected from the top of the third layer, applying a shift at the interface.

Shift of layer (km)	Time−RMS (s)
0.0	0.043
−0.2	0.048
0.2	0.052
−0.4	0.047
0.4	0.069
−1.0	0.089
1.0	0.113

RMS traveltime increases strongly if the shift is greater than 400 m. Thus the errors in depth for reflecting horizons can be estimated to within a few hundred metres. The second test involved a stepwise increase of the velocity at four nodes of the second layer (Table 4). The velocity is strongly constrained: a variation of 0.2 km s^{-1} clearly reduces the quality of the fit.

The reliability of the model was also quantified during the inversion procedure, where estimates of the resolution and of the absolute parameter uncertainties were calculated (Zelt & Smith 1992). The diagonal elements of the resolution matrix

Table 4. RMS traveltime residual (Time−RMS) with respect to the observed data, calculated for rays reflected from the top of the third layer, applying a stepwise increase of the velocity of four nodes of the second layer.

Variation of velocity (km s^{-1})	Time—RMS (s)
0	0.047
0.2	0.081
0.4	0.140

range between zero and one (Fig. 10). A value close to unity indicates a well-resolved parameter; a low value ($\ll 1$) denotes a poorly resolved parameter. The resolution presented in Fig. 10 is that obtained when all the parameters are inverted together. In practice, the inversion was carried out progressively, step by step, first for the shallower layers and then for the deeper layers. The resolution shown in Fig. 10 indicates the worst case. The resolution actually obtained in the stepwise inversion process is better. As expected, the velocity resolution in the two first layers is good (greater than 0.5 for most of the velocity nodes) and decreases at greater depth. Nevertheless, the resolution is consistently good in the central part of the model. The resolution of the depth of the layers is lower. This result is comparable to the results obtained by Zelt & Smith (1992). A comparison of Figs 8 and 10 shows that the resolution computed by the Zelt program compares well with the uncertainties estimated by our empirical check.

GRAVITY MODELLING

The most striking feature of the Bouguer anomaly map in southwestern Ireland is the pronounced low near Killarney (Fig. 11, Murphy 1960). This gravity low, mainly orientated east–west, continues westwards from the large anomaly associated with the Leinster Granite (e.g. Readman, O'Reilly & Murphy 1997). The gravity profile along the seismic line is shown in Fig. 12(a) and crosses the western part of the Killarney gravity low.

An initial gravity model was obtained by converting the seismic velocities to density, following the Nafe & Drake (1957) and Christensen & Mooney (1995) relationships. The uppermost, thin layer in the seismic model was not included in the gravity model as the gravity data coverage is not adequate to resolve such fine detail. The MacRay program (Luetgert 1992) was used to compute a 2-D gravity model using Talwani's
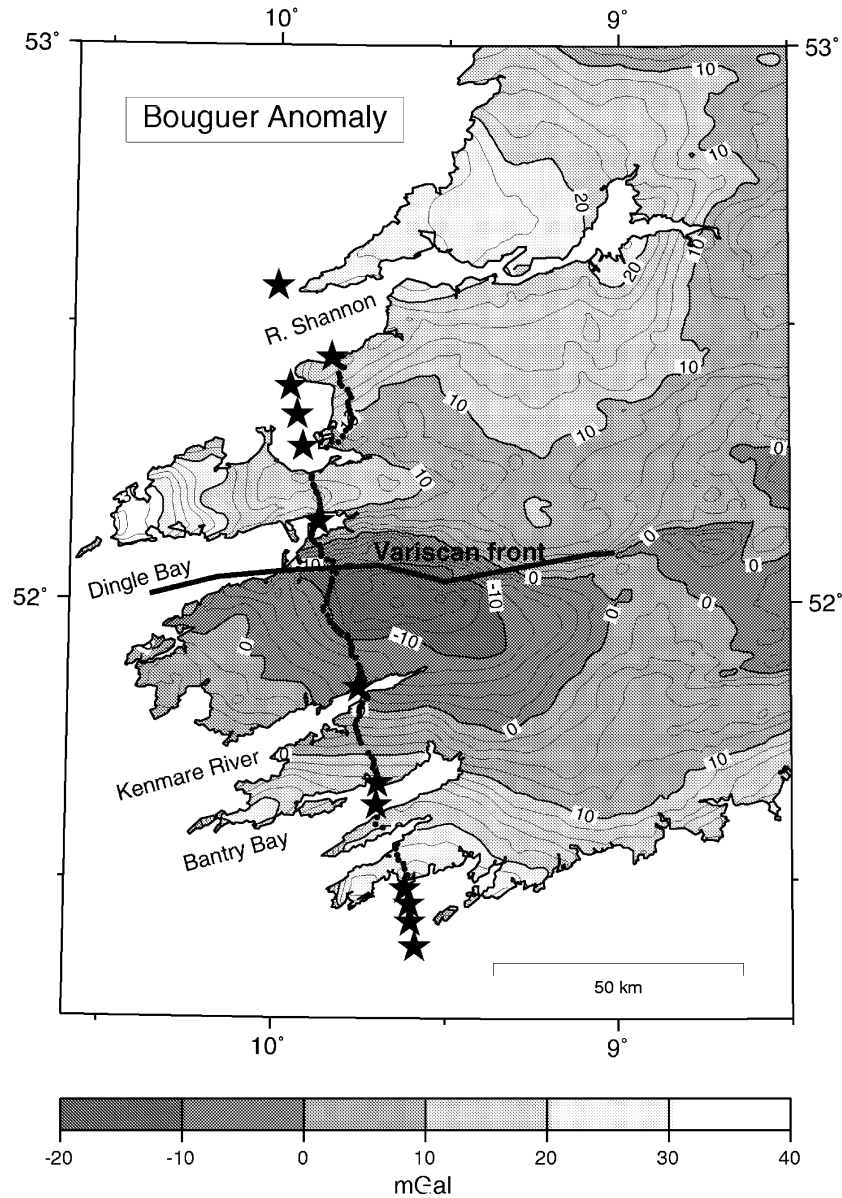
Figure 11. Bouguer anomaly map for southwest Ireland. Contour interval 2 mgal, Bouguer density 2670 kg m^{-3}. Data from the Dublin Institute for Advanced Studies (e.g. Murphy 1960; Readman *et al.* 1997). The location of the seismic profile is indicated.

method (Talwani, Worzel & Landisman 1959). One of the main features of the velocity model is the low-velocity zone located in the upper crust between about 75 and 85 km. However, neither its extent nor its density derived directly from the Nafe–Drake curve is adequate to explain fully the magnitude and extent of the gravity anomaly. It is necessary to extend the zone to the south and reduce its density to obtain a satisfactory fit with the observed anomaly (see dotted line in Fig. 12a).

The geometry shown in Fig. 12 requires the density to be reduced to 2600 kg m^{-3} within a zone where the seismic velocities range from 5.43 to 6.04 km s^{-1}. This density is low compared to the measured densities of approximately 2650 kg m^{-3} for Irish granites published by Morris (1973). However, a recent comprehensive programme of measurements from both core and surface samples of the Caledonian Leinster Granite in southeast Ireland indicates a range of bulk densities

from 2590 to 2670 kg m^{-3} (O'Brien, personal communication). This lends confidence to our density assumption. The density values for sedimentary rocks published by Morris (1973) are higher than this value. The depth to the Moho is not well constrained by the seismic data at the southern end of the profile, and a better regional fit to the gravity data is obtained if this depth is slightly reduced compared to the seismic model. Otherwise the geometry of the layers in the gravity model is the same as that in the seismic model (see Figs 8 and 12).

An important factor is that the seismic profile does not pass directly over the centre of the gravity low. Therefore, an alternative and more plausible explanation for the observed anomaly is that the profile passes over the low-density body close to its western boundary, making the approximation to a 2-D structure no longer valid. The gravity model thus inferred from the seismic velocity structure would then not match the structure of the proposed granite, whose dimensions probably
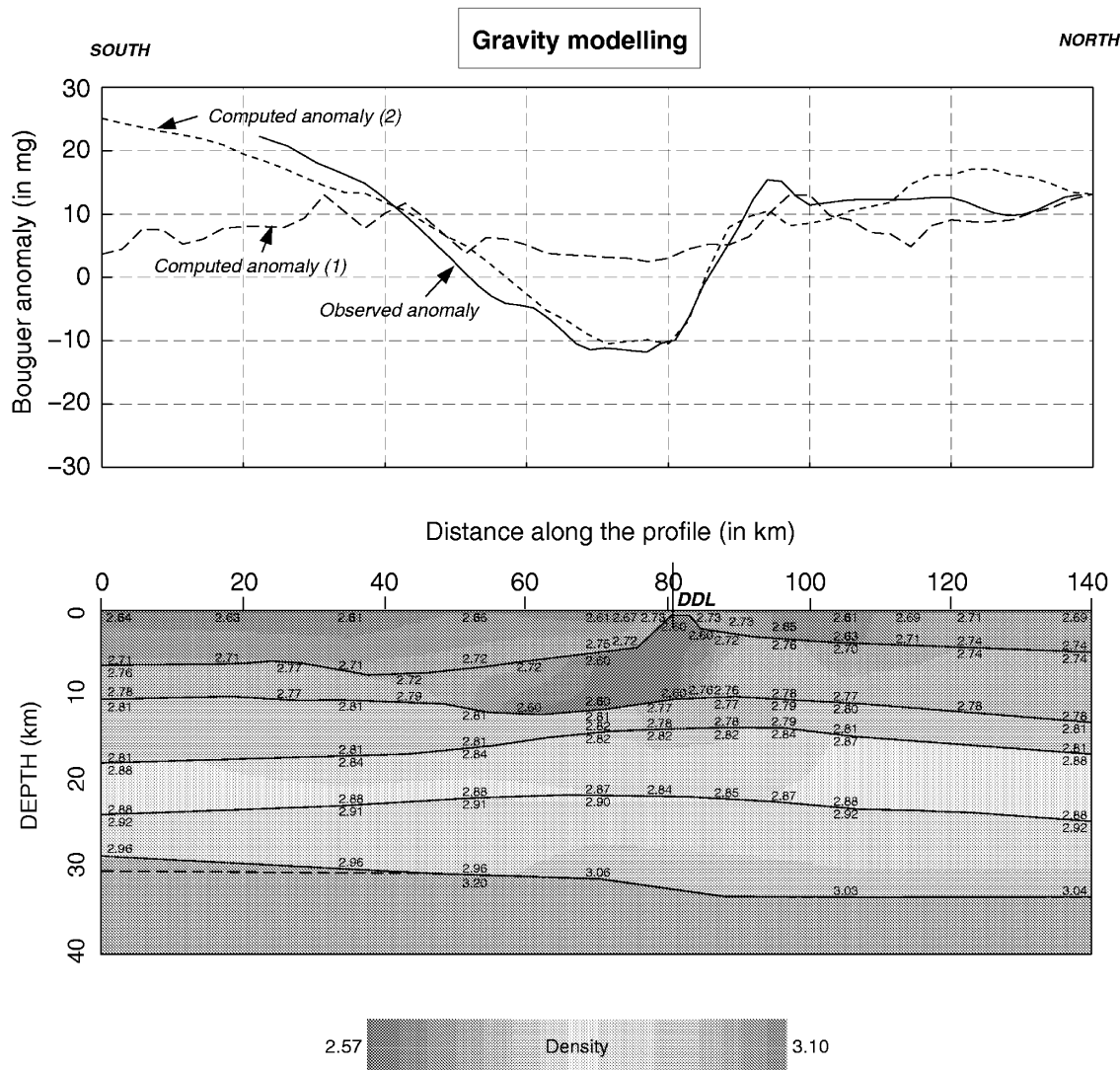
Figure 12. (a) Computed and observed gravity anomalies. The continuous line shows the observed anomaly and the dashed line (1) shows the computed anomaly from the densities deduced from the Nafe–Drake relationship. The dotted line (2) is the computed anomaly from the model with an extended low-density zone and a decrease of the Moho depth. (b) Density model deduced from the velocity model using the Nafe & Drake (1957) conversion curve, including an extended low-density zone (2600 kg m^{-3}) and a decrease of the Moho depth in the south.

increase to the east of the profile. 3-D gravity modelling and additional gravity measurements will be necessary to test this explanation fully.

GEOLOGICAL AND TECTONIC INTERPRETATION

Sediments and upper crust

The wide-angle model demonstrates considerable lateral thickness and velocity changes within the upper-Palaeozoic sedimentary succession and the upper crust along the profile (see seismic and gravity models, Figs 8 and 12). Some of these variations in the upper part of the succession are well constrained by the surface geology (Fig. 2).

The upper layer south of the DDL is generally of the order of 6–7 km thick. It reaches a maximum thickness in the region to the north of Bantry Bay and gradually thins northwards towards the southern edge of Dingle Bay. It coincides with the thick Munster Basin and is interpreted as upper-Palaeozoic strata consisting mainly of non-marine red-bed sandstones and shales. A number of large Variscan synclinal cores contain Late Devonian to Tournaisian marine facies overlying the thick Devonian succession. The low-velocity package immediately north of 28 km coincides with the Bantry Bay syncline and may reflect one such package of lower-velocity Carboniferous shale-prone sediments. To the north of the DDL (approximately 84 km), the interpreted upper-Palaeozoic succession is considerably thinner and reaches a maximum thickness of 4 km. The velocity of the layer increases suddenly north of 112 km. This is likely to reflect the increased thickness of high-velocity Tournaisian limestones and Namurian clastics in the area north from Kerry Head, in comparison with the Devonian clastics of the Slieve Mish anticline in the Dingle peninsula.

The upper-crustal layer (layer 2) is 3–4 km thick at the south of the profile but is approximately 8 km thick to the north of the DDL. Its base lies at a depth of approximately

10–12 km. While the variable thicknesses within the sedimentary layer and the underlying upper-crustal layer could perhaps be the result of a complex pattern of thin-skinned thrust duplexes, the consistent pattern of thick sediments overlying correspondingly thin upper crust is compatible with a sedimentary response to extension and crustal thinning. The thin nature of the upper crust along the southern part of the profile may reflect crustal extension and thinning during the syn-rift development of the Devonian Munster Basin. The more uniformly thick crust to the north of the DDL probably represents relatively unstretched crust to the north of the Munster Basin, where the thinner sedimentary succession largely comprises a thermal subsidence sequence in the sense described by McKenzie (1978).

A pronounced low-velocity zone occurs near 80 km within the upper-crustal layer, which is roughly coincident with a major Bouguer anomaly low (see Figs 11 and 12). This has been variously modelled and interpreted either as a sedimentary depocentre or, by analogy with the coincidence of similar anomalies with known granite outcrops in Ireland, as a granite body (Howard 1975; Ford *et al.* 1991). The incompatibility of the velocities derived from the wide-angle profile with the likely densities of sedimentary strata at this level makes it improbable that the anomaly is caused by a sedimentary body. Instead, the data are suggestive of the presence of a granitic body. The gravity anomaly derived from the seismic model beneath the profile using 2-D modelling would not be expected to agree exactly with the observed anomaly if the granite was more extensive to the east of the profile, as is suggested by the shape of the anomaly. The gravity anomaly, mainly orientated east–west, lies immediately to the west of the NE–SW extension of the anomaly associated with the Leinster Granite (Readman *et al.* 1997). It appears to change strike from NE–SW to more of an E–W orientation as it extends beneath the upper-Palaeozoic sediments of the Variscan terrane.

The role of the granite in Variscan structuring

The granite proposed in the model is a relatively shallow, largely upper-crustal feature. It is broadly similar in its structural level (with a base of 10 km) to the granite model proposed for the region on the basis of gravity data by Ford *et al.* (1991), and to the granite proposed along-strike to the east by Lowe & Jacob (1989). It is likely to be a Caledonian feature which was emplaced in Early Devonian times and is part of a complex of similar-aged granites which extends from SE Ireland across into North America. As a buoyant body within the upper crust, its southern margin, or its metamorphic aureole, may have served as a structural focus for the development of the northern margin of the fault-controlled Munster Basin. It is also suggested that the granite acted as a buffer or obstacle to northward-directed Variscan thrusting. This may have caused the amalgamation of a series of flat-lying thrusts within the sedimentary succession and upper-crustal layer, and the ramping to the surface of the composite thrust. Unfortunately, the resolution of the present seismic data is insufficient to distinguish the subtle velocity variations that would result from stacked thrust sheets within a sedimentary or upper-crustal layer (layers 1 and 2). However, the wide-angle model would appear to confirm the suggestion of Meere (1995) that the geometry and structure of the southwestern part of the Irish Variscides were determined largely by a combination of the stratigraphic succession in the Munster Basin and the obstacle effect of a major igneous batholith.

The problem of the middle crust

Two mid-crustal layers are observed in the model. The upper one thins from approximately 8 km south of 50 km to less than 4 km further north. It displays a generally constant velocity gradient, with a slight decrease beneath the proposed granite. The lower layer shows a reversed, albeit more subdued, thickness pattern, being thicker in the north. Again, there is a slight velocity decrease beneath the upper-crustal low-velocity zone.

Meere (1995) has suggested a Variscan thrusting model with major faults soling out at depths of 19–22 km. This coincides approximately with the base of the upper mid-crustal layer. The thicker crust (layer 3) to the south of the proposed granite and of the DDL could therefore be explained as resulting from the stacking of thrust packages involving a crustal component. However, this thin-skinned model (i.e. thrust faults with a linking horizontal detachment) fails to explain easily the observed northward thickening within the lower middle crust (layer 4). The thickening lies to the north of the Variscan front in an area where the surface geology gives no indication of significant structural shortenings comparable to that in the thrust zone. A more plausible explanation is that the thickness variations within the two layers of the middle crust represent an inherited Caledonian feature. In this case, Variscan thrusting was likely to have been confined to the sedimentary succession and part of the crust. The granite, together with the northern boundary of the Munster Basin, was thus located above a deep-seated Caledonian structural feature.

The somewhat diffuse lower-velocity areas within the middle-crustal layers, underlying the proposed granite, are suggested as being related to the formation of the granite. They may represent either a deeper root to the granite, or a fractured mid-crustal sequence which facilitated upward granite migration.

The lower crust and the link with shallow structures

The major features beneath the mid-crustal layers are the southward thinning of the lower crust, the step in the Moho and the location of a high-velocity zone above it, located between about 50 and 100 km. The low-velocity zone in the upper crust is located directly above the high-velocity zone. It is tempting to speculate on the possible connection between these features. Two interpretations are suggested. (1) The thickening and the high-velocity zone may represent crustal underplating of Caledonian age, whose thermal effects may have induced mid-crustal melting and the generation of the granite. This could account for the thinning of the 6.03–6.08 km s^{-1} layer in this area. (2) The high-velocity material may represent the residue from lower-crustal melting that produced the granite which then rose to intrude the upper-crustal (Caledonian) metasediment. However, some thinning of the lower-crustal layer might be expected in the latter case and does not appear to be present. The first explanation is therefore favoured. Lowe & Jacob (1989) observed a similar southward thinning of the lower crust and a resultant gradual rise in the Moho on the COOLE line further east. Murphy (1981) observed a gravity rise towards the coasts around

Ireland and suggested a gradual crustal thinning from the centre of the country towards the coast. While these authors did not propose an explanation, the observation that the thinning occurs in areas other than the south coast suggests that it is unlikely to be related to the formation of the Munster Basin. The fact that Ireland is virtually surrounded by relatively young extensional sedimentary basins (Shannon 1991) indicates that the feature may be a far-field, deep crustal response to Mesozoic extension in the Irish offshore regions.

CONCLUSIONS

A preliminary model of a wide-angle profile across the Variscides in SW Ireland shows a number of important features which have implications for the geological development of the region. The following are the main features of the model.

(1) Five velocity layers have been defined. An upper-Palaeozoic sedimentary layer 5–8 km thick is present. This is underlain by an upper-crustal layer of variable thickness, with a base generally at a depth of 10–12 km. Two mid-crustal layers are defined, and a lower-crustal layer below 22 km. The Moho lies at a depth of 30–32 km.

(2) An upper-crustal low-velocity zone is observed in the central part of the region. This coincides with a well-defined gravity low and is modelled as a Caledonian granite which intruded upper-crustal basement. The granite may have acted as a buffer to northward-directed Variscan thrusting.

(3) The Dingle–Dungarvan Line (DDL) marks a major change in sedimentary and crustal velocity and in structure. It is broadly coincident with the gravity low, and with thickness and velocity differences in many of the underlying layers down to the Moho. This suggests a deep, pre-Variscan control of the structural development of this area.

(4) The velocity structure derived is compatible with, but does not conclusively prove, a thin-skinned tectonic model of linked thrust faults soling into a horizontal detachment. The upper-Palaeozoic sediments and varying amounts of the crust may be involved in such deformation.

ACKNOWLEDGMENTS

REFERENCES

Christensen, N.I. & Mooney, W.D., 1995. Seismic velocity structure and composition of the continental crust: a global view, *J. geophys. Res.,* **100,** 9761–9788.

Cooper, M.A., Collins, D.A., Ford, M.A., Murphy, F.X. & Trayner, P.M., 1984. Structural style, shortening estimates and the thrust front of the Irish Variscides, in *Variscan Tectonics of the North Atlantic Region,* eds Hutton, D.H.W. & Sanderson, D.J., *Geol. Soc. Lond. Spec. Publ.,* **14,** 167–176.

Cooper, M.A., Collins, D., Ford, M., Murphy, F.X. & Trayner, P.M., 1986. Structural evolution of the Irish Variscides, *J. geol. Soc. Lond.,* **143,** 53–63.

Emenike, E.A., 1986. An interpretation of the Killarney and Leinster gravity anomalies in the Republic of Ireland, *Ir. J. Earth Sci.,* **7,** 125–132.

Ford, M., Brown, C. & Readman, P., 1991. Analysis and tectonic interpretation of gravity data over the Variscides of southern Ireland, *J. geol. Soc. Lond.,* **148,** 137–148.

Gill, W.D., 1962. The Variscan Fold Belt in Ireland, in *Some Aspects of the Variscan Fold Belt,* pp. 49–64, ed. Coe, K., Manchester University Press, Manchester.

Howard, D.W., 1975. Deep-seated igneous intrusions in Co. Kerry, *Proc. R. Ir. Acad., 75 B,* 173–183.

Jacob, A.W.B., Vees, R., Braile, L.W. & Criley, E., 1994. Optimization of wide-angle seismic signal-to-noise ratios and *P*-wave transmission in Kenya, in *Crustal and Upper Mantle Structure of the Kenya Rift,* eds Prodehl, C., Keller, G.R. & Khan, M.A., *Tectonophysics,* **236,** 61–80.

Lowe, C. & Jacob, A.W.B., 1989. A north–south seismic profile across the Caledonian Suture zone in Ireland, *Tectonophysics,* **168,** 297–318.

Luetgert, J.H., 1992. MacRay—Interactive two-dimensional seismic raytracing for the Macintosh, *USGS Open File Rept,* 92–356.

McKenzie, D., 1978. Some remarks on the development of sedimentary basins, *Earth planet. Sci. Lett.,* **40,** 25–32.

Matte, P., 1986. Tectonic and plate tectonics model for the Variscan belt of Europe, *Tectonophysics,* **126,** 329–374.

Meere, P.A., 1995. The structural evolution of the western Irish Variscides: an example of obstacle tectonics?, *Tectonophysics,* **246,** 97–112.

Morris, P., 1973. Density, magnetic and resistivity measurements on Irish rocks, *Communications of the Dublin Institute for Advanced Studies, Geophysical Bulletin,* Series D, **31.**

Murphy, T., 1960. Gravity anomaly map of Ireland, sheet 5—South West, *Dublin Institute for Advanced Studies, Geophysical Bulletin,* **18.**

Murphy, T., 1974. Gravity anomaly map of Ireland, *Dublin Institute for Advanced Studies, Geophysical Bulletin,* Series D, **32.**

Murphy, T., 1981. Geophysical evidence, in *A Geology of Ireland,* pp. 225–229, ed. Holland, C.H., Scottish Academic Press, Edinburgh.

Nafe, J.E. & Drake, C.L., 1957. Variation with depth in shallow and deep water marine sediments of porosity, density and the velocities of compressional and shear waves. *Geophysics,* **22,** 523–552.

Price, C.A. & Todd, S.P., 1988. A model for the development of the Irish Variscides, *J. geol. Soc. Lond.,* **145,** 935–941.

Readman, P.W., O'Reilly, B.M. & Murphy, T., 1997. Gravity gradients and upper-crustal tectonic fabrics, Ireland, *J. Geol. Soc. Lond.,* **154,** 817–828.

Sanderson, D.J., 1984. Structural variation across the northern margin of the Variscides in NW Europe, in *Variscan Tectonics of the North Atlantic Region,* eds Hutton, D.H.W. & Sanderson, D.J., *Geol. Soc. Lond. Spec. Publ.,* **14,** 149–166.

Shannon, P.M., 1991. The development of Irish offshore sedimentary basins, *J. geol. Soc. Lond.,* **148,** 181–189.

Talwani, M., Worzel, J. & Landisman, M., 1959. Rapid gravity computations for two dimensional bodies with application to the Mendicino submarine fracture zone, *J. geophys. Res.,* **64,** 49–59.

Williams, E.A., Bamford, M.L.F., Cooper, M.A., Edwards, H.E., Ford, M., Grant, G.G., MacCarthy, I.A.J., McAfee, A.M. & O'Sullivan, M.J., 1989. Tectonic controls and sedimentary response in the Devonian–Carboniferous Munster Basins, south-west Ireland, in *The Role of Tectonics in Devonian and Carboniferous Sedimentation in the British Isles,* eds Arthurton, R.S., Gutteridge, P. & Nolan, S.C., *Yorkshire Geological Society Occasional Publication, 6,* 123–141.

Zelt, C.A. & Smith, R.B., 1992. Seismic traveltime inversion for 2D crustal velocity structure, *Geophys. J. Int.,* **108,** 16–34.